JOURNAL OF MATERIALS SCIENCE 27 (1992) 1663–1671

Interfacial studies on carbon/thermoplastic model composites using laser Raman spectroscopy

L. S. SCHADLER, C. LAIRD
Department of Materials Science and Engineering, University of Pennsylvania, 3231 Walnut Street, Philadelphia, PA 19104, USA

N. MELANITIS, C. GALIOTIS
Department of Materials, Queen Mary and Westfield College, University of London, Mile End Road, London E1 4NS, UK

J. C. FIGUEROA
E. I. Du Pont de Nemours and Co. Inc., Experimental Station, P.O. Box 80304, Wilmington, DE 19880, USA

Interfacial studies were carried out on a model composite system consisting of a short carbon fibre embedded in a polycarbonate matrix. While the composite was being strained, the local strain along the fibre was monitored using a Raman spectroscopic technique. The residual compressive strain in the fibre due to fabrication was found to be -0.45%. Subsequent loading of the composite up to 0.55% in tension resulted in a complex stress field consisting of tension at the fibre ends and compression in the middle of the fibre. The fibre strain at different levels of applied load was converted to interfacial shear stress (ISS) distribution along the fibre by employing a simple equilibrium analysis. The shape of the ISS profiles indicated a predominantly frictional type of load transfer from the matrix to the fibre. Finally, the maximum ISS value of 15 MPa was found to be unaffected by the amount of strain experienced by the composite.

1. Introduction

It is now well established that the integrity of the fibre/matrix interface has a strong influence upon the efficiency of stress transfer in polymer matrix composites [1–4]. In turn, composite properties such as compressive strength and toughness, as well as off-axis properties [2, 5–7] can be considerably affected by the stress-transfer efficiency at the interfacial level. A useful model system for studying the stress transfer from the matrix to the fibre is a mono-filament composite system because fibre–fibre interaction is eliminated, and the interface can be carefully controlled to yield reproducible results. Mono-filament composites have been used by many groups to study the monotonic behaviour of the interface in graphite/thermoset composites [2, 4, 9–11], but by only a few groups to study the monotonic behaviour of the interface in thermoplastic composites [1, 12–14]. Thermoset matrix composites are the most widely used polymer composites, but thermoplastic matrix composites have been developed in recent years for several reasons: thermoplastics can be extrusion moulded, they can be remelted and remoulded for in-the-field repairs, they are less hygroscopic than most thermosets, and in some cases can maintain their properties at high temperatures [15].

A Raman spectroscopic technique was developed recently that uses fibres as strain sensors in a composite to map the strain along a fibre, and to determine locally the load transfer behaviour [16, 17]. This Raman technique has been used to study several systems including Kevlar [18, 19] and carbon/epoxy [17] systems, and has been extended here to study interfacial behaviour of short filaments embedded in a thermoplastic matrix (polycarbonate). The paper reports measurements of the residual strain produced in the monofilament, and the subsequent build up of load in the fibre with applied composite tensile strain. The distribution of interfacial shear stress (ISS) calculated at several strain levels is also reported.

2. Background

Interfacial behaviour in single filament composites is often studied by breaking the fibre with a longitudinal load (thus creating a free surface) and by observing the subsequent transfer of load from the matrix to the fibre through an interfacial shear stress (ISS). The interfacial shear stress (ISS), τ, can be related to the axial stress in the fibre, σ, by a force equilibrium analysis of a single fibre loaded in a composite (Fig. 1).

0022–2461

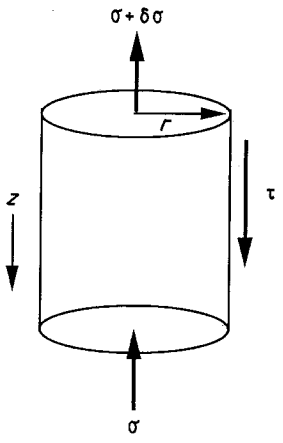

$$\sigma\pi r^2 + 2r\pi\tau\delta z = (\sigma+\delta\sigma)\pi r^2$$

Figure 1 Force equilibrium diagram of a single fibre loaded in a composite.

The resulting equilibrium equation is [20]

$$\sigma\pi r_o^2 + 2\pi\tau r_o dz = \pi r_o^2(\sigma + \delta\sigma) \quad (1)$$

where z is the distance along the fibre, and r is the fibre radius. In order to derive an expression for the interfacial shear stress (ISS) from this equation, several approaches have been followed. The shear lag model [20] assumes (a) perfect bonding at the interface, (b) no load transfer through the fibre ends, and (c) no stress concentrations near the fibre ends. The boundary conditions are, in fact, zero stress at the fibre ends, and an inter-fibre distance of $2R$. Given a fibre of length, L, loaded to a strain e, Cox [20] found that the stress distribution in the interface region is proportional to the fibre, and matrix moduli, the length of the fibre, and the inter-fibre spacing, R. In the case of single-fibre composites, R is difficult to determine, and can be used as a variable to fit single filament experimental data to the Cox model [11], but has been estimated to be 5.2 times the fibre radius [21].

Equation 1 can be solved by calculating the average interfacial shear stress [14] (the average shear stress is equal to the shear stress integrated over the distance, L, divided by L), or by assuming that the shear stress is constant [22, 23]

$$\tau = (\sigma r)/2L \quad (2)$$

where L is the length of the fibre in which load is transferred from the matrix to the fibre (the transfer length). The interfacial shear stress can then be measured experimentally by measuring a stress parameter and a length parameter. The length parameter is called the critical length, L_c, defined as the length at which the fibre is short enough that the axial stress in the fibre cannot build up to the failure stress of the fibre. The stress parameter is the fibre failure stress at the length L_c (see Fig. 3 below) [1, 2, 4, 8, 13, 24]. The difficulty with this technique is that the fragment lengths can vary from L_c to $L_c/2$ and the strength of a fibre varies along its length requiring complicated statistical analysis to obtain the length and strength parameter.

To eliminate the use of statistics for the fibre strength and fragment length distributions, a new optical fragmentation technique was developed [14] that replaces the failure strength with the applied strain multiplied by the modulus of the fibre, and the critical length with the transfer length at strains well below the critical strain (see Fig. 2). This technique also yields an average interfacial shear stress.

An improvement over the above optical fragmentation techniques for obtaining interfacial shear stress distributions is the Raman spectroscopic technique [11]. By solving Equation 1 exactly, the ISS distribution along a fragment can be calculated instead of an average ISS [17]. The advantages of measuring an ISS distribution over an average ISS is that the maximum ISS can be determined, and the shape of the distribution can yield information about whether the mechanism of load transfer is due to friction, matrix yielding, or good bonding.

Raman spectroscopy probes the atomic vibrations of crystalline materials. When an external load is applied the equilibrium interatomic distance changes, and thus the interatomic force constants which determine the frequency of atomic vibrations also change. This results in a shift in the Raman peaks with applied strain. Therefore, by measuring the magnitude of this shift, one can convert Raman frequency into strain in the same way that electrical resistance is converted to strain in the resistive strain gauges. It has been shown

$$\tau = (\delta\sigma/\delta z)\, r/2 \quad ; \quad \frac{{}_0\int^{L} \tau\,\delta z}{L} = \sigma r/2z \Big|_0^L$$

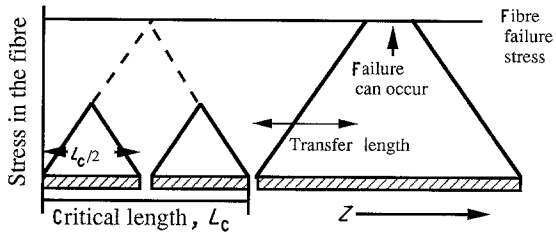

(a) $\overline{\tau} = \sigma_{failure}\, r/2L_c$

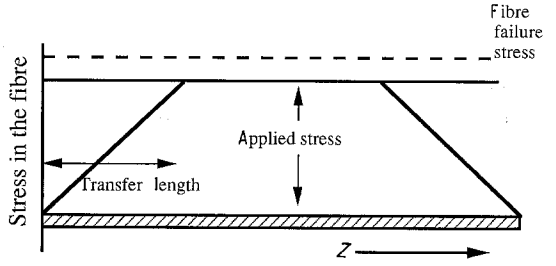

(b) $\overline{\tau} = \sigma_{applied}\, r/2L_{\text{transfer length}}$

Figure 2 (a) Schematic drawing of the stress distribution in a few fibre fragments showing an example of critical length, (b) an example of a technique for measuring the transfer length and the strain in the fibre.

that in graphite fibres the shift in the Raman peak with applied strain is linear and sensitive enough for strain measurements [25, 26]. The shift in the Raman peak is calibrated by loading a bare filament in a micro-extensometer, and measuring the peak shift as a function of applied strain. The strain of an embedded fibre in a transparent matrix can then be mapped along its length [17].

This technique is a powerful tool for micromechanical studies of the interface. If the strain in the fibre can be mapped along the fibre length, then the build up of load in the fibre can be measured as a function of distance; Equation 1 can be solved exactly to yield a distribution in ISS along a fibre length [17]

$$\tau(z) = [d\varepsilon(z)/dz](E_f r/2) \quad (3)$$

where E_f is the Young's modulus of the fibre.

The Raman shift with strain is termed the Raman frequency-gauge factor (RFGF) and is a measure of the sensitivity of the fibres as a strain gauge. The tensile RFGF has been measured for graphite fibres of different moduli, and it has been found that the RFGF increases with fibre modulus [27]. The compressive RFGF has also been measured for graphite fibres of varying modulus using a cantilever beam technique [27]. The compressive RFGF was found to be less than the tensile RFGF, and the difference between the tensile and compressive RFGF increased with decreasing modulus in graphite fibres.

The Raman technique has been used to perform a traditional fragmentation test in Kevlar® fibre/epoxy matrix short-fibre model composites, and the strain and ISS distributions have been mapped [11, 18, 19]. Good bonding was found at low strains, and the Cox's shear lag prediction was found to fit the data reasonably well. At higher composite strains, the interface began to fail resulting in an ISS that is due to frictional load transfer, and is lower than the ISS due to good bonding [11].

The advantages of a short fibre is that the strain distribution can be mapped from the fibre end at any strain level. In this study short graphite fibres are embedded in polycarbonate, and the strain distribution is mapped from 0.0–1.1% strain. This allows the build up of strain in the fibre from compression to tension to be monitored, and the ISS distributions to be calculated at each strain level.

3. Experimental procedure

3.1. Materials

The PAN-based graphite fibre used in this programme is a Hercules HMS-4 fibre. The matrix material is General Electric Lexan® polycarbonate ($T_g = 140\,^\circ C$). The monofilament composites were prepared in a mould by placing cleaned fibres, secured on each end, between two sheets of cleaned and dried polycarbonate 0.25 mm thick. The mould was heated to 190 °C between two platens at a heating rate of 3 °C min^{-1} under a pressure of 3900 Pa, and was air cooled. Upon cooling, the fibre was loaded in compression because of the large difference in the coefficients of thermal expansion between the fibre and the matrix. The compressive strain was high enough to cause a shear failure in the fibre during cooling. The shorter fibres so produced remained aligned because the temperature at which they failed was low enough that the matrix could not flow considerably. Tensile samples (9.5 mm × 75 mm × 0.5 mm) were cut from the moulded sheet.

3.2. Raman/interfacial studies

Raman spectra were taken with an argon-ion laser with a wavelength of 514.5 nm and a power of 2 mW. A modified Nikon microscope was used to focus the incident beam to a spot size as small as 2 μm. The 180° backscattered light was collected by the microscope objective and focused on the entrance slit of a SPEX 1877 triple monochromator. A cooled charge coupled device (CCD) imaging detector recorded the Raman spectra.

The shift of the E_{2g} Raman peak maxima ($\sim 1580\,cm^{-1}$) in tensile strain was measured by stretching the fibres with a modified micrometer. The shift of the E_{2g} Raman peak in compression was measured using a cantilever beam technique [27] where the fibre is mounted on a cantilever beam and the beam is flexed to compress the fibres. The Raman peak maximum was found by subtracting the matrix background peak from the whole spectra, and then fitting the remaining fibre spectra using a Lorentzian fit.

The single-filament composites were displaced using a mini-tensile testing device. The composite strain was measured with a strain gauge mounted directly in the gauge length.

The error in fibre strain measurements was estimated from the variability in the wavenumber measured at a given point in the fibre, and the variability in the RFGF. The error in ISS was estimated from the variation in slope that occurred given the variation in strain.

4. Results

4.1. Raman shift

The Raman spectra for the E_{2g} vibrational mode for Hercules HMS-4 at 0.0% and 1.1% applied strain are shown in Fig. 3. The peak at 0.0% strain is at $\sim 1580\,cm^{-1}$. Fig. 4 shows the continuous shift of the Raman peak with applied tensile strain for two fibres. The shift is linear over the entire range and has a negative slope of $-8.5 \pm 0.3\,cm^{-1}$ per 1% strain. This value is consistent with that measured for other graphic fibres of similar modulus [17]. The compressive RFGR was predicted based on previous studies of fibres of various moduli [28], and is estimated to be $-7.3\,cm^{-1}$ per 1% strain.

4.2. Residual strain in the composite

Because of the large difference in the coefficient of thermal expansion (CTE) between the fibre and the matrix, after the moulding is cooled, there are residual stresses in the sample. The state of strain in the sample

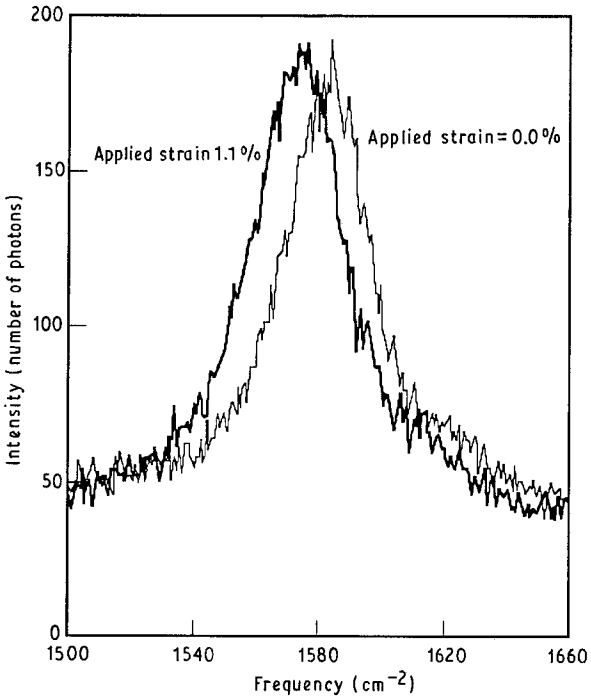

Figure 3 Typical Raman spectra for HMS-4 at 0.0% and 1.1% strain.

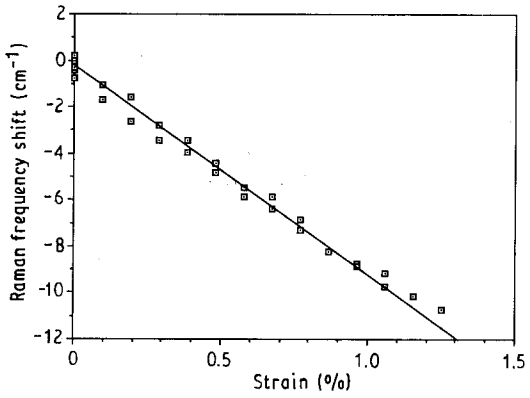

Figure 4 Raman frequency as a function of strain for the 1580 cm^{-1} band of HMS-4.

was quantified; the fibre was assumed to be a transversely isotropic linear elastic material, and the matrix an isotropic non-linear material. The CTE of polycarbonate and of graphite was assumed to be constant below the glass transition temperature, T_g (140 °C). The sample was cooled from T_g to room temperature (25 °C). The CTE of polycarbonate is higher above T_g than below it, but because there is considerable flow of the matrix above the glass transition temperature, the applied strain on the fibre above T_g was assumed to be zero. If the matrix modulus was held constant from the glass transition temperature to room temperature, the bulk matrix strain was -0.8% compression. The axial strain on the HMS was also calculated to be -0.8% compression. The radial and hoop stress and strain distributions are shown in Fig. 5. The radial strain in the fibre is constant and small, but the matrix is in radial compression close to the fibre, reaching zero load, and the bulk shrinkage strain at a distance

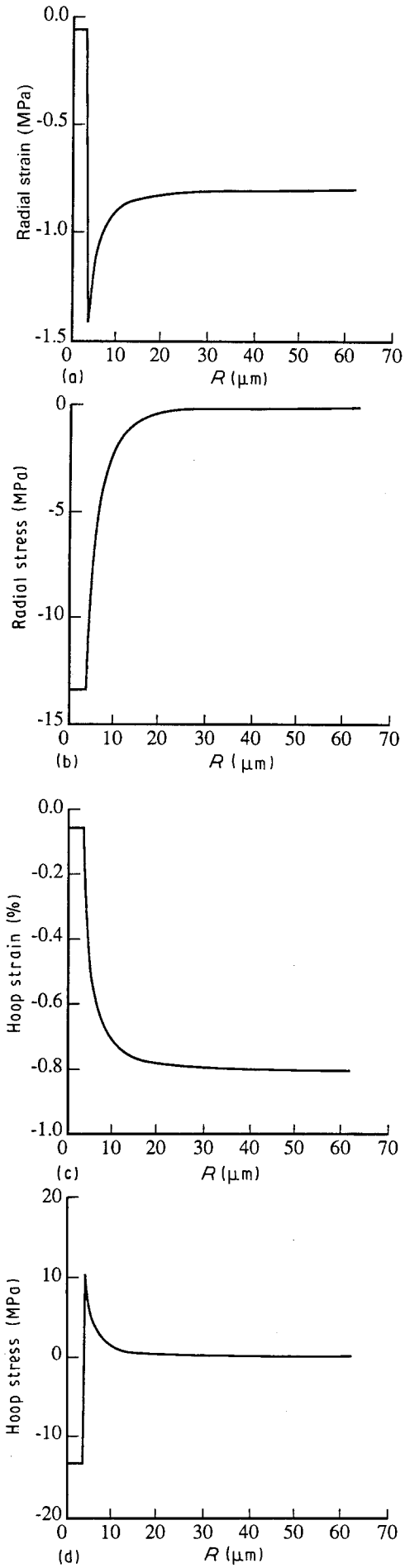

Figure 5 (a) The radial strain as a function of radius, (b) the radial stress as a function of radius, (c) the hoop strain as a function of radius, (d) the hoop stress as a function of radius. The fibre radius is 3.5 μm.

of a few fibre diameters from the interface. Therefore, the interface is in radial compression. The hoop strain on the fibre is also small and compressive, while the hoop stress in the matrix is tensile. Although the magnitude of the strain values would vary by assuming some flow below T_g, the sign of the strain would remain the same.

As load is applied to the composite, the axial strain decreases, but Poisson's effects increase the radial and hoop stress in compression except for the matrix hoop stress which increases in tension.

4.3. Strain mapping

The strain in the embedded fibre was monitored from 0.0%–1.1% applied composite strain. Fig. 6a–d depict the strain in the fibre as a function of distance from the fibre end. The fibre is initially in axial compression; the average strain in the centre of the fragment is 0.45% compressive strain. As the applied strain is increased to 0.22%, the end of the fibre is loaded in tension, but the centre of the fibre fragment remains in compression. By 0.55% applied composite strain the fibre is almost entirely in tension, but the fibre ends are carrying more strain than the centre of the fibre. At 1.1% strain the fibre strain builds continuously from the end of the fibre to the centre.

4.4. Interfacial studies

The interfacial shear stress (ISS) was calculated from the strain–distance curves by calculating the slope, de/dz, at each point and using Equation 3. The slope was determined by fitting a second-order polynomial to 11 points of the data of strain versus distance data at one time using a least-squares-fit and, then, by calculating the derivative at the centre point. The effect of varying the number of points for each fit from 7–13, and the order of the polynomial from second to third order was minimal. The calculated ISS for four strains, 0.0%, 0.22%, 0.55%, and 1.1% is shown in Fig. 7a–d. The sign of the shear reflects the sign of the slope of strain with distance; the change in sign of ISS is important, but the initial reference sign is arbitrary. The change in sign of the ISS represents a change in the slope of the axial stress build up in the fibre; in order to maintain equilibrium, the integrated shear stress must equal zero, so there is both positive and negative shear along the fibre. The maximum ISS observed is about 18 MPa. The maximum ISS is relatively constant with applied strain except that the maximum ISS for 0.22% applied strain is only 10 MPa. This may be because the change of the sign of the shear in the maximum region masks the higher ISS. The maximum ISS is much less than the yield stress of the matrix (50 MPa) implying that the load transfer is due to friction. When 0.55% strain is applied to the composite, a given transfer length experiences both positive and negative shear reflecting the build up of load near the fibre end, and the eventual drop in load some distance along the fibre. By 1.1% strain, the strain builds continuously in the fibre, and the sign of the shear stress is again constant within a given transfer length.

4.5. SEM studies

To help determine the mechanism of load transfer, scanning electron micrographs of bare fibres, and fibres that had been embedded in polycarbonate, were compared. The micrographs are shown in Fig. 8. The HMS bare fibre and the fibre pulled from the matrix

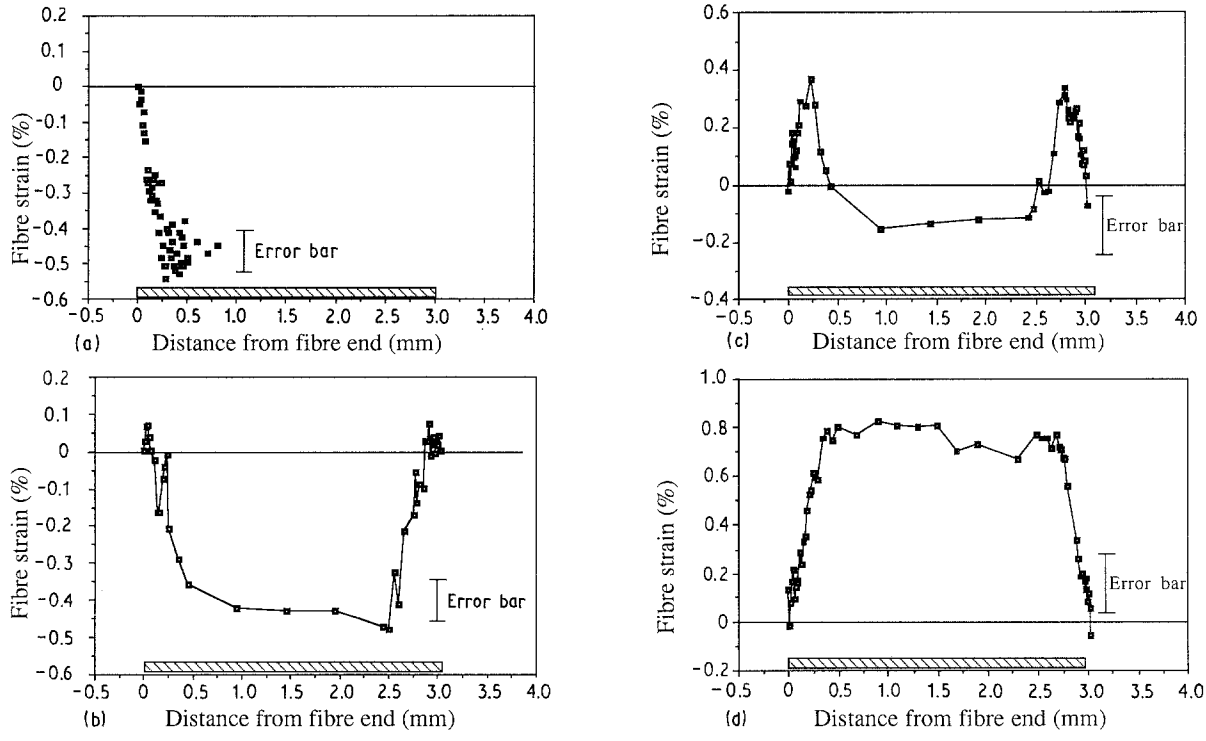

Figure 6 Typical profiles of fibre strain as a function of fibre length for various applied strains. (a) 0.0%, (b) 0.22%, (c) 0.55%, (d) 1.1%.

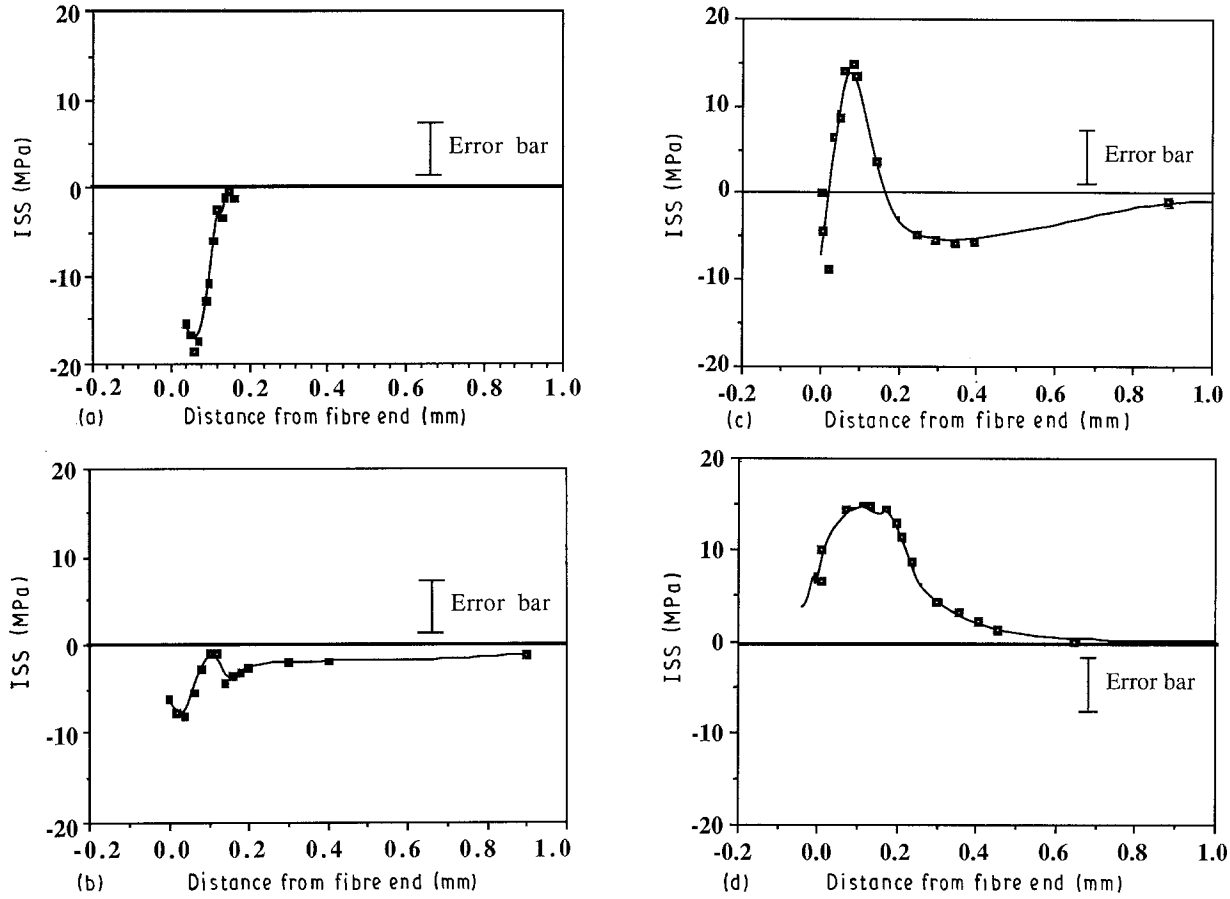

Figure 7 Typical profiles of the ISS of HMS at several strain levels: (a) 0.55% applied strain, (b) 1.1% applied strain, (c) 1.67% applied strain, (d) 2.22% applied strain.

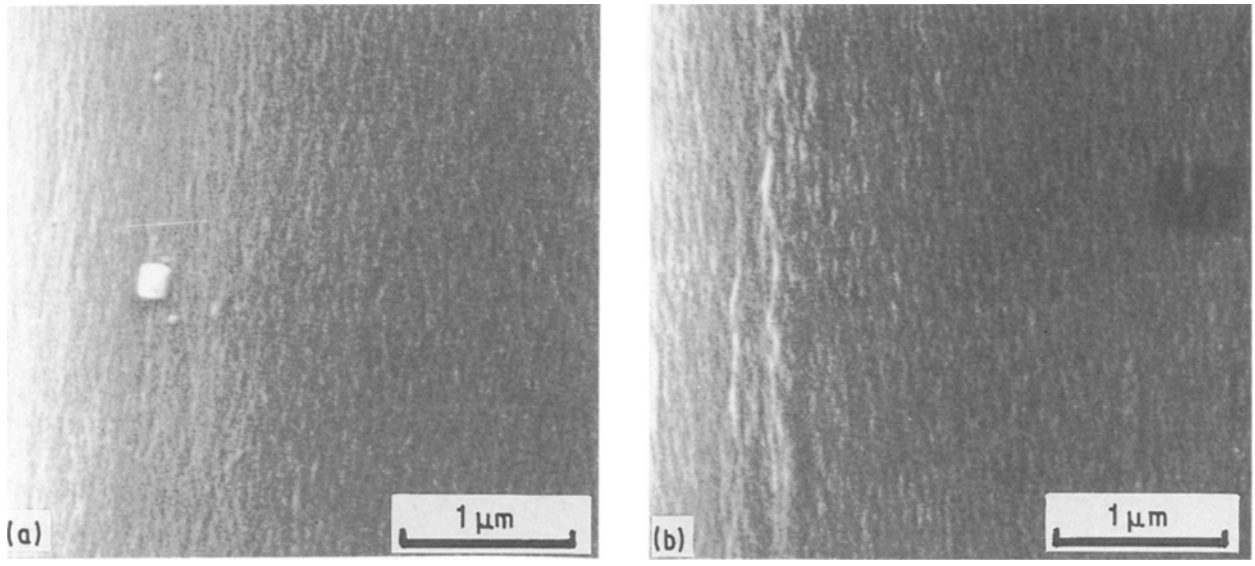

Figure 8 Typical scanning electron micrographs comparing (a) a bare HMS fibre with (b) a fibre pulled from the matrix.

have similar surfaces. This suggests that the failure occurred directly along the fibre matrix interface, supporting the observation that the load transfer mechanism in HMS/PC is a frictional load transfer.

5. Discussion

5.1. Strain mapping

When a thermoplastic matrix composite is cooled, the difference in coefficient of thermal expansion creates residual stresses. Raman spectroscopy has already been used to measure the compressive strain on graphite fibres in pre-pregs, and the strain in the fibres was found to be as predicted analytically [29]. In single filament composites, however, the volume fraction of fibre is so low that the matrix contracts as much as it would if the fibre were not present, and as a result the fibre is loaded into higher compression [7].

For HMS in polycarbonate the calculated strain in the fibre is -0.8% strain. However, HMS fails by brittle shear at 0.55% compressive strain. The mean maximum compressive strain of $-0.45\% \pm 0.1\%$ is not incongruous with the predicted strain, because when the fibre failed during fabrication the strain may have been relieved.

If a Cox-model prediction of a fibre loaded to -0.45% strain, a radius of influence, or interfibre spacing, of $5.2r_0$ [21] is compared to the data, the fit is good only at higher strains as shown in Fig. 9. The slope of the strain versus distance plot is slightly lower than predicted by the Cox model, and no further comparisons between the shape of the strain profiles can be made due to the large scatter in the data. If the data are compared to a frictional model that predicts a constant shear stress, the fit is good at lower strains, but deviates from the model at strains close to the maximum strain. The constant shear stress value was determined by fitting a straight line to the first 11 points of data.

The subsequent build up of load in the fibre as tensile strain is applied to the sample results in a more complicated state of stress in the fibre. As tensile strain is added to the composite, the fibre is under a three-dimensional compressive field on the top of which an axial tensile force is applied. Adding a tensile strain places the region near the fibre end in tension because the compressive strain was not as large near the end, and reduces the compressive strain in the centre of the fibre, but does not eliminate it. Neither model can predict this behaviour; however, if the model behaviour is superimposed on the experimental data, the results are interesting. Fig. 10 shows a plot of the experimental data of 0.22% applied strain, and the fibre strain predicted by both the Cox shear lag model, and the frictional model if 0.3% strain is applied to the composite. A comparison of the experimental data at

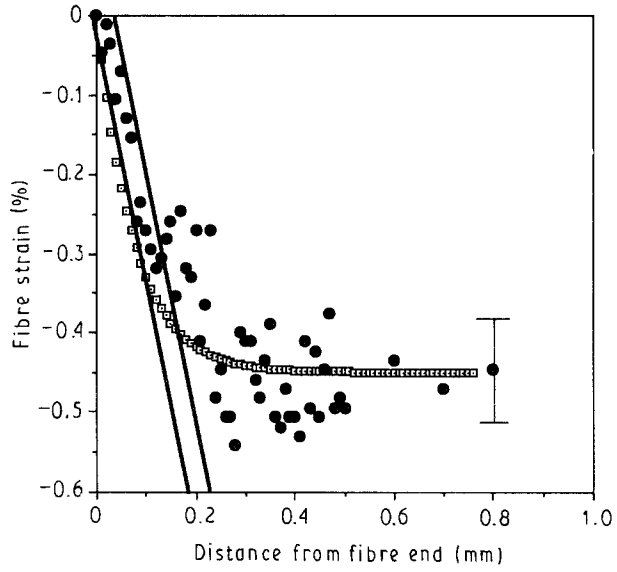

Figure 9 Comparison of (●) experimental data with those predicted by (□) Cox's solution to the shear lag analysis, and with (—) the linear frictional model at 0.0% applied strain.

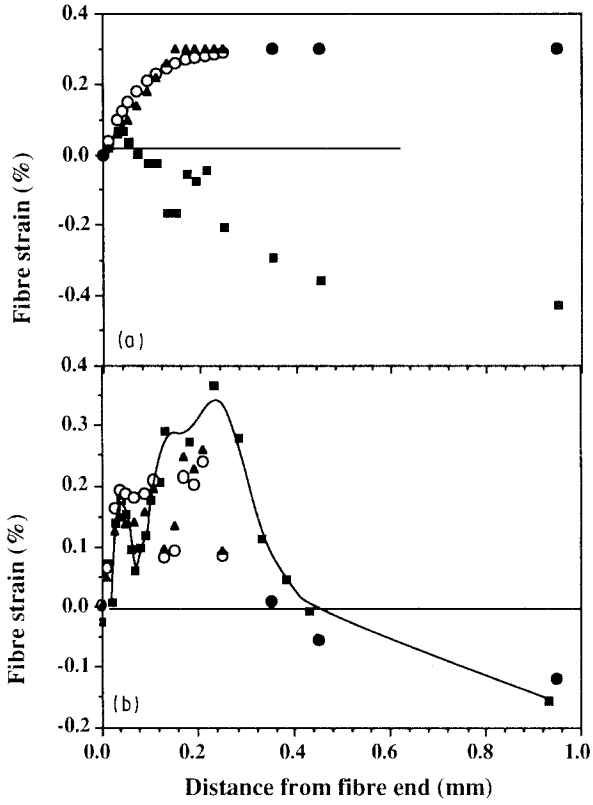

Figure 10 (a) (■) 0.2% Experimental data, and (○) the Cox shear lag solution for 0.3% as well as (—) the linear frictional model for 0.3% applied strain. (b) A comparison of (■) the 0.5% experimental data with the 0.22% experimental data superimposed with an additional 0.3% calculated from (○) the Cox shear lag model and (▲) the linear frictional model.

0.55% applied strain is compared to a superposition of the experimental 0.22% data and the 0.3% model behaviour in Fig. 10b. The superposition does not match the experimental data at 0.55% closely. However, there are some similarities. The centre of the fibre in both cases experiences an increase of 0.3% applied strain. Secondly, the cross-over point from tension to compression is the same for both distributions. In addition the various dips in the experimental strain are observed in the superposition. The differences in the predicted and experimental data are significant. The experimental data reaches a maximum of 0.4% strain, and the superposition only reaches 0.27% strain; therefore some portions of the fibre gained 0.5% strain when only 0.33% strain was applied. In addition, the model predicts that the strain builds more quickly near the fibre end than is observed.

The inability of linear models to predict the behaviour in the stress transfer zone (STZ), especially the non-linear build up of strain, is not clear at this point in the study, but is also not surprising given the complicated state of stress in the fibre. If the shear stress in the stress transfer zone were higher at higher strains, then an increase in fibre strain higher than the applied strain could be explained because the stress in the fibre is just the shear stress integrated over distance. However, this is not the case as evinced by the constant maximum shear stress at several applied strain levels.

5.2. Interfacial studies

The ISS distribution found is indicative of a frictional load transfer mechanism. The maximum value of 15 MPa is well below the yield stress of polycarbonate, and remains constant throughout the loading sequence. Typical values of frictional load transfer are 10 MPa [11]. The larger value observed in this system may be due to the radial stresses introduced during processing or due to a higher coefficient of friction. The constant value throughout the loading sequence implies that the additional radial strain placed on the fibre during loading due to Poisson's effects does not affect the frictional load transfer.

Fig. 11 is a model of the development of the ISS distribution in one-half of a fragment as strain is applied to a composite. At 0.0% applied strain, the strain in the fibre builds from 0.0% at the fibre end to a compressive strain, and is constant in the centre of the fragment. The ISS in the stress transfer zone, for the sake of argument is taken as negative. In the region of constant fibre strain, the ISS is zero. As strain is applied to the composite there is both a positive and negative ISS in the stress transfer zone. In the region adjacent to the fibre end, the fibre strain builds from 0.0% at the end to a positive value; the ISS is positive in this region. At some distance along the fibre, the strain in the fibre begins to decrease; the ISS is negative in this region. The cross-over point from positive to negative shear moves away from the fibre end until the applied strain is high enough that the fibre increases in strain continuously from the fibre end until it reaches a constant value. At this applied strain, the ISS in the stress transfer zone is positive throughout the entire stress transfer zone.

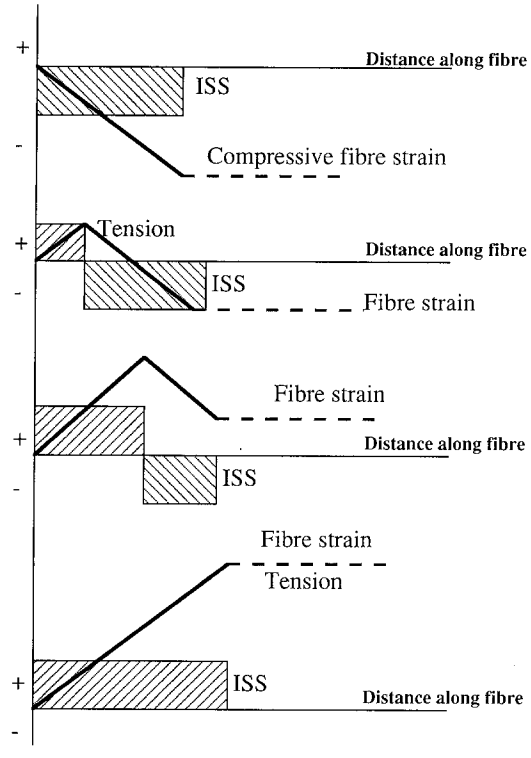

Figure 11 Schematic drawing of the change of sign of shear as the fibre is loaded from compression to tension.

6. Conclusions

The above study on the interfacial behaviour of HMS short-fibre polycarbonate matrix composites using a Raman spectroscopic technique lead to the following conclusions.

1. The residual strain in HMS/polycarbonate single filament composites is great enough to fail the HMS fibre in compressive shear during moulding. The resulting residual strain is $-0.45\% \pm 0.1\%$.
2. The load transfer in HMS/polycarbonate is primarily frictional load transfer, and is not affected by Poisson's ratio effects.
3. The build up of load in the fibre from compression to tension results in a complicated state of stress and strain in the fibre that cannot be modelled with current models.

Acknowledgements

The work was part of a collaborative project between the University of Pennsylvania, and Queen Mary and Westfield College. L. Schadler acknowledges the support of the E. I. Du Pont de Nemours and Co. Inc. and The University of Pennsylvania, Laboratory for Research on the Structure of Matter under Grant no. DMR-88-19885. N. Melanitis thanks the Science and Engineering Council and the Royal Aerospace Establishment for a scholarship grant. We are grateful for the support and for the excellent assistance of A. L. Radin, B. D. Campbell and L. L. Peterson. Discussions with Z. Hashin were invaluable.

References

1. L. DILANDRO, A. T. DIBENEDETTO and J. GROEGER, *Polym. Compos.* **9** (1988) 209.
2. L. T. DRZAL, *Adv. Polym. Sci.* **75** (1986) 1.
3. P. EHRBURGER and J. B. DONNET, *Phil. Trans. R. Soc. Lond. A* **294** (1980) 495.
4. A. N. NETRAVALI, L. T. T. TOPOLESKI, W. H. SACHSE and S. L. PHOENIX, *Compos. Sci. Technol.* **35** (1989) 13.
5. J. L. KARDOS, *J. Adhesion* **5** (1973) 119.
6. S. W. TSAI and H. T. HAHN, *Polym. Sci. Technol.* **12B** (1980) 463.
7. D. H. KAELBLE, *J. Adhesion* **5** (1973) 245.
8. J. NAIRN and P. ZOLLER, *J. Mater. Sci.* **20** (1985) 355.
9. W. D. BASCOM and R. M. JENSEN, *J. Adhesion* **19** (1986) 219.
10. F. J. McGARRY and M. FUJIWARA, in "23rd Annual Technical Conference 1968 of Reinforced Plastics Division, The Society of the Plastics Industry" (SPI, 1968) p. 1.
11. C. GALIOTIS, *Compos. Sci. Technol.* **42** (1991) 125–150.
12. A. T. DiBENEDETTO, L. NICOLAIS, L. AMBROSIO and J. GROEGER, "Proceedings of the 1st International Conference on Composite Interfaces (ICCI-I)", Cleveland, OH, edited by H. Ishida and J. L. Koenig (Elsevier, New York, 1988).
13. J. C. FIGUEROA, L. S. SCHADLER, and C. LAIRD, in "Proceedings of the Materials Research Society Symposium", November 1989, Boston MA, edited by C. G. Pantano and E. J. H. Chen (1989) p. 000.
14. L. S. SCHADLER, J. C. FIGUEROA and C. LAIRD, *ibid.*, p. 345.
15. R. C. TENNYSON, T. A. WATERHOUSE, S. NEWMAN and M. T. TAKEMORI, *Polym. Compos.* **6** (1982) 437.
16. C. GALIOTIS, R. J. YOUNG, P. H. J. YEUNG and D. N. BATCHELDER, *J. Mater. Sci.* **21** (1983) 2483.
17. N. MELANITIS, P. TETLOW, C. GALIOTIS and C. K. L. DAVIES, in "Interfacial Phenomenon in Composite Materials '89", edited by F. R. Jones (Butterworths, Sheffield, 1989) p. 97.

18. H. JAHANKHANI and C. GALIOTIS, in "Interfaces in Polymer, Ceramic, and Metal Matrix Composites", edited by Ishida (Elsevier Science, New York, 1988) pp. 107–181.
19. H. JAHANKHANI and C. GALIOTIS, *J. Compos. Mater.* **25** (1991) 609–631.
20. H. L. COX, *Brit. J. Appl. Phys.* **72** (1952).
21. G. P. CHEREPANOV, in "Mechanics of Brittle Fracture" (McGraw-Hill International, New York, 1979) p. 616.
22. A. KELLY and W. R. TYSON, *J. Mech. Phys. Solids* **13** (1965) 329.
23. J. O. OUTWATER Jr, *Modern Plastics* **33** (1956) 156.
24. L. T. DRZAL, M. J. RICH, M. F. KOENIG and P. F. LLOYD, *J. Adhesion* **16** (1983) 133.
25. I. M. ROBINSON, M. ZAKIKHANI, R. J. DAY, R. J. YOUNG and C. GALIOTIS, *J. Mater. Sci. Lett.* **6** (1987) 1212.
26. C. GALIOTIS and D. N. BATCHELDER, *ibid.* **7** (1988) 545.
27. N. MELANITIS and C. GALIOTIS, *J. Mater. Sci.* **25** (1990) 5081.
28. C. GALIOTIS, N. MELANITIS and H. JAHANKHANI, in Proceedings of I. Mech. E., FRC'90, "Fibre Reinforced Composites", University of Liverpool (1990) p. 81.
29. C. FILIOU and C. GALIOTIS, in "Deformation and Fracture of Composites" (Plastics and Rubber Institute, UK, 1991) pp. 20–I.

Received 9 May
and accepted 17 May 1991